Volume 54
Number 29
7 August 2025
Pages 11115-11452

Dalton Transactions

An international journal of inorganic chemistry

rsc.li/dalton

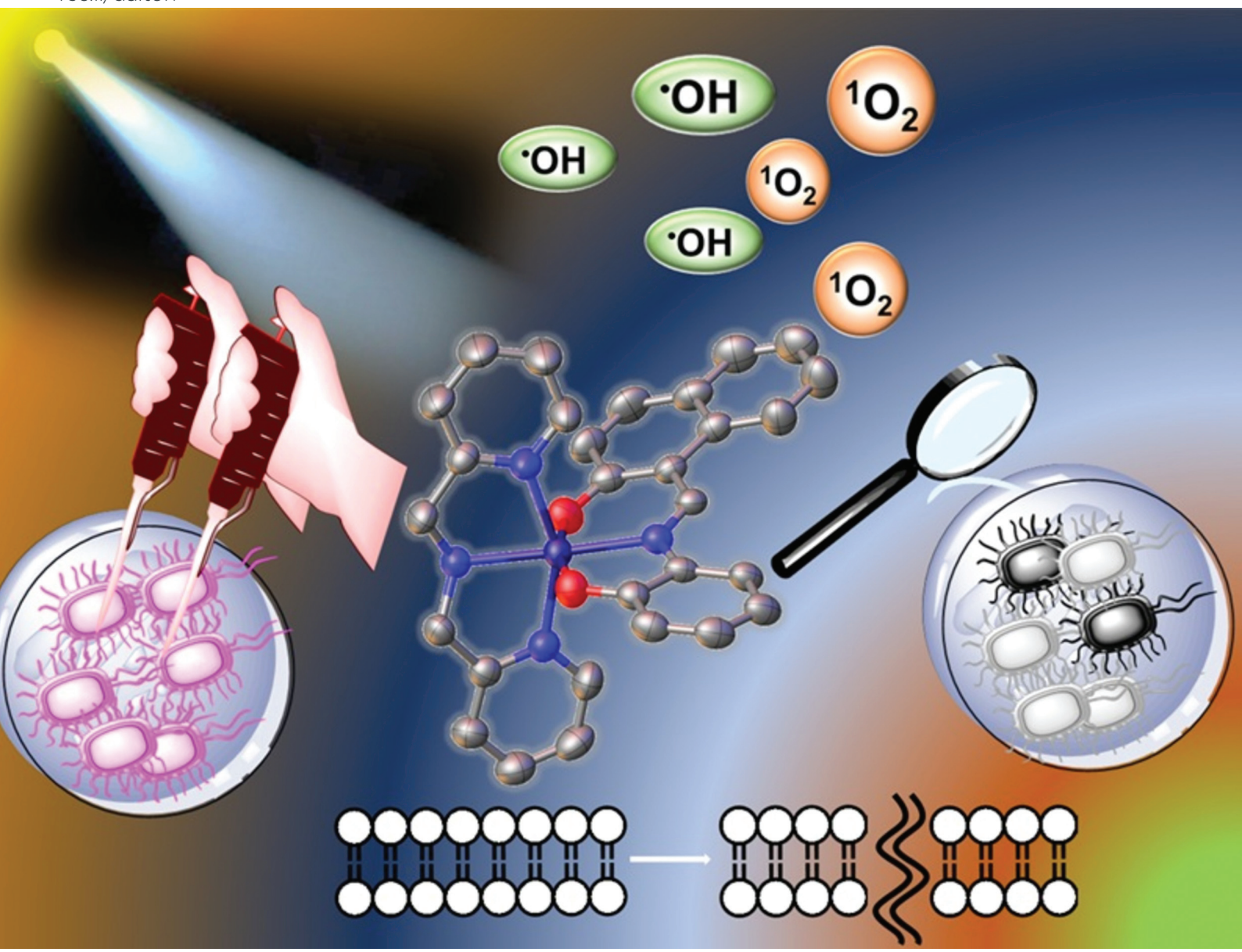

ISSN 1477-9226

ROYAL SOCIETY OF CHEMISTRY

PAPER

Samya Banerjee *et al.*

Photoactivated antibacterial activity of Fe(III) complexes *via* singlet oxygen-mediated bacterial membrane lysis

Dalton Transactions

ROYAL SOCIETY OF CHEMISTRY

PAPER

View Article Online
View Journal | View Issue

Cite this: *Dalton Trans.*, 2025, **54**, 11174

Photoactivated antibacterial activity of Fe(III) complexes *via* singlet oxygen-mediated bacterial membrane lysis†

Ishwar Singh,[a] Rohit Rai,[b] Rajesh Kushwaha, [a] Prodyut Dhar *[b] and Samya Banerjee *[a]

In this work, four novel Fe(III) complexes *viz.*, [Fe(dpa)(L1)]Cl (**Fe1**), [Fe(Fc-dpa)(L1)]Cl (**Fe2**), [Fe(dpa)(L2)]Cl (**Fe3**), and [Fe(Fc-dpa)(L2)]Cl (**Fe4**), where dpa = bis(2-pyridylmethyl)amine; Fc-dpa = *N*-(1-ferrocenyl)-methyl-1-(pyridine-2-yl)-*N*-(pyridine-2-ylmethyl)methanamine; H_2L_1 = (*E*)-2(2-hydroxybenzylidene) amino)phenol and H_2L_2 = (*E*)-1-(2-hydroxyphenyl)imino)methyl)naphthalen-2-ol, have been synthesized and characterized. The light-responsive nature of these complexes was tailored by extending π conjugation or attaching a ferrocene moiety in the ligands. These complexes displayed light absorption within the visible region with λ_{max} ~ 450 nm. X-ray structures of **Fe3** revealed a distorted octahedral structure around the Fe(III) center with a FeN_4O_2 core. Further, the frontier molecular orbitals (FMOs) and adiabatic energy splitting between excited states were determined by DFT calculations. **Fe1–Fe4** did not demonstrate any notable antibacterial action without light. Nevertheless, the antibacterial effect of **Fe1–Fe4** was significantly increased due to their $^1O_2$ generation ability under light conditions. Interestingly, the MIC value of **Fe1–Fe4** was observed to be *ca.* 0.2 μg mL^{-1} against *S. aureus* and 0.5 μg mL^{-1} against *E. coli*. under light exposure. The light-induced antibacterial activities of these complexes were attributed to bacterial cell membrane damage *via* reactive oxygen species (ROS) generation. Overall, this study presents the first report of Fe(III) complexes showing antibacterial activity under visible light conditions.

Received 3rd June 2025,
Accepted 30th June 2025

DOI: 10.1039/d5dt01300c

rsc.li/dalton

Introduction

Antibacterial resistance has emerged as one of the most concerning public health challenges, affecting healthcare globally.[1–3] In 2019, bacterial infections were the second leading death-causing disease, *ca.* 7.7 million deaths worldwide.[4,5] O'Neill's report warned that if no action is taken, this figure could rise dramatically, leading to approximately 10 million deaths annually by 2050.[5–7] The severity of antibacterial resistance on global health can be compared to the combined effects of influenza, tuberculosis (TB), and HIV/AIDS.[4,5] Therefore, novel treatment approaches and antibacterial agents are urgently needed to address antibacterial resistance.[8–10] In this context, antibacterial photodynamic therapy (aPDT) is one of the promising new antibacterial strategies due to its non-invasiveness, minimal adverse effects, and ability to avoid drug resistance.[8–11] The main mechanism of action (MoA) of aPDT against bacteria includes the activation of photosensitizers (drug molecules) at the target infection site to produce reactive oxygen species (ROS) upon light exposure.[12–14] The produced ROS rupture the bacterial internal structure and oxidatively damage the bacterial biofilm, increasing the death factor and ultimately causing bacterial cell death.[11–14] In general, aPDT overcomes the limitation of conventional antibacterial agents by providing a novel mechanism of action that kills bacteria under the influence of light by inducing oxidative stress.[9,11,15] Moreover, selective light irradiation at the target infection site reduces potential side effects or harm to unexposed healthy cells.[15,16] In this regard, cyanine dyes, porphyrin systems, and organic compounds have been explored as aPDT agents.[17–19] However, their poor bioavailability and stability hinder their potential for aPDT applications.[15,20] Recently, metal-based photosensitizers caught significant attention due to their stability, rich photophysical/photochemical properties, and tunable excited state properties.[20–26] For example, Hohlfeld and coworkers reported the phototoxic activity of photostable heteroleptic dipyrrinato

[a]*Department of Chemistry, Indian Institute of Technology (BHU), Varanasi, Uttar Pradesh 221005, India. E-mail: samya.chy@itbhu.ac.in*
[b]*School of Biochemical Engineering, Indian Institute of Technology (BHU), Varanasi, Varanasi, Uttar Pradesh, 221005 India. E-mail: prodyut.bce@iitbhu.ac.in*

†Electronic supplementary information (ESI) available. CCDC 2455812. For ESI and crystallographic data in CIF or other electronic format see DOI: https://doi.org/10.1039/d5dt01300c

Ir(III) complexes against *S. aureus* and *P. aeruginosa*, being non-toxic towards normal human cells.[27] Zhang and coworkers reported three-photon responsive Pt(II) complexes for aPDT application by targeting DNA and L-lysine of *S. aureus* bacterial strain.[28] Smitten group reported the light-responsive antibacterial effect of Os(II)-based complexes against methicillin-resistant *S. aureus* (MRSA) and *E. coli*.[29] Our group showed the efficacy of polypyridyl Ru(II) complexes in inhibiting bacterial growth and biofilm disruption under visible light exposure.[30] Although heavy metal-based complexes have shown promising results as therapeutic aPDT agents, they might still suffer from the inherent toxic effects of the heavy metals.[31–33] Therefore, the focus has shifted toward developing 3d metal-based aPDT agents, as they are bio-essential and biocompatible.[20,34,35] Our group recently explored the aPDT applications of several 3d metal-based complexes.[36–39] The curcumin-based Co(II) and Zn(II) complexes presented promising bacterial growth inhibition under visible light exposure, being non-toxic to normal cells.[36,38,39] Ferrocene and vitamin B6-derived Co(III) complexes presented concentration-dependent antibacterial efficacy against both Gram-negative and Gram-positive bacteria under light conditions.[37] So far, very limited reports are available for first-row transition metal complexes as photoactivated antibacterial agents, and therefore, there is a timely need to explore other metal complexes to broaden the scope of this research field.[11,36–39] Iron is a bio-essential element for human health due to its involvement in different important biological processes.[11,39] Iron complexes have been reported to inhibit bacterial growth significantly.[11,41–43] For example, Scott *et al.* have discovered that the flexicate system of Fe(II) complexes interacts specifically with DNA and demonstrated antibacterial activity against MRSA and *E. coli*.[41] Tovmasyan and coworkers have also shown bacterial growth inhibition against *S. aureus* and *E. coli* bacteria by Fe(II) complexes under dark conditions.[42] In a comparative study conducted by the Gust group among the Schiff-base complexes of Zn(II), Mn(III), Ni(II), and Fe(II)/(III), iron complexes presented higher antibacterial activity against *S. aureus* and MRSA.[42] Despite several iron complexes being explored as antibacterial agents under dark conditions, Fe(III) complexes for aPDT application have not been reported so far.

The discovery of ferrocene has been a milestone in organometallic as well as in medicinal chemistry following the realization of its therapeutic potential.[44,45] It contained several favourable properties, including electron transfer, enhanced lipophilicity, improved bioavailability, *etc.*[44,45] Ferrocene has been incorporated into several clinical/preclinical known anticancer and antimalarial drugs improve their efficacy and overcome drug resistance problem.[44–48] For example, the ferrocene derivative of tamoxifen has presented much better anticancer activity against breast cancer than its parent drug.[46] Similarly, a ferrocene derivative of chloroquine, *i.e.*, ferroquine, has undergone phase II clinical trials for effective malaria treatments. Besides, ferrocene has also been conjugated in different heterometallic compounds to improve their anticancer potential.[44,49] For example, the Gasser group and Metzler-Nolte group have incorporated a ferrocene moiety in rhodium complexes and achieved cisplatin-like anticancer effect against prostate cancer cells with a different mode of cell death.[50,51] Similarly, the Patra group has also identified the potency of ferrocene pendants in Pt(II)/Ru(II) complexes for improved anticancer activity.[52,53] The Chakravarty group has exploited the ferrocene-based absorption in the green to red light region to produce selective light-triggered anticancer activity against different cancer cells by attaching it with different metal cores, *e.g.*, Pt, V, Cu, *etc.*[54–57] Recently, our group has also observed an increase in light-triggered antibacterial activity of Co(III) complex upon ferrocene conjugation.[37]

Based on the above background, herein, four novel visible light-responsive Fe(III) complexes (**Fe1–Fe4**) (Fig. 1a) have been explored for aPDT application. Photoactive dipicolylamine (dpa) and ferrocenyl-dipicolylamine (Fc-dpa) were used as tridentate-N,N,N donor ligands to bring photo-responsiveness to the complexes. Additionally, O,N,O-donor Schiff bases were used to facilitate ligand-to-metal charge transfer (LMCT) transitions in the visible region and to modulate the lipophilicity of the resulting Fe(III) complexes. In **Fe2** and **Fe4**, the attached ferrocenyl moiety can potentially bring a bimetallic-specific MoA, and being redox active, can produce higher ROS. In addition, ferrocene is also known to exhibit antifungal, antibacterial, antimalarial, and anticancer activities.[37,44–57] **Fe1–Fe4** presented significant $^1O_2$ generation under visible light exposure. Further, the light-triggered antibacterial efficacy of **Fe1–Fe4** was determined against Gram-negative (*E. coli*) and Gram-positive (*S. aureus*) bacteria with or without light exposure.

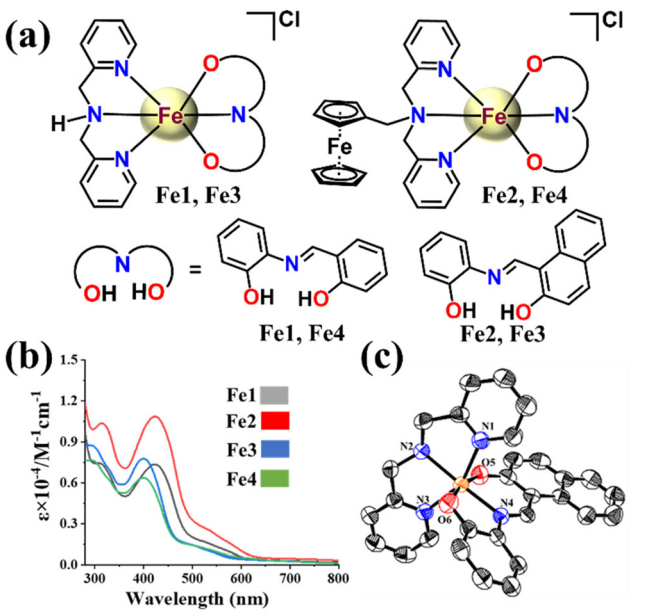

Fig. 1 (a) Structures of **Fe1–Fe4**. (b) UV-Vis. spectra of **Fe1–Fe4** in LB media–DMSO (99 : 1 v/v). (c) ORTEP diagram of cationic **Fe3** with 50% thermal ellipsoid probability. Hydrogens and ClO_4^- are omitted for clarity.

Results and discussion

Synthesis and characterization

Four novel Fe(III)-based complexes, *viz.*, **Fe1–Fe4**, were synthesized in optimal yield. **Fe1–Fe4** were synthesized according to Schemes S1, ESI.† The trichloride salt of Fe(III) was added to the methanolic solution of N,N,N donor ligand at ambient temperature, followed by the addition of the methanolic solution of deprotonated Schiff base. **Fe1–Fe4** were characterized with spectroscopic techniques, including HRMS, FT-IR, SC-XRD, and UV-Vis. spectroscopy (Fig. 1a–c, and Fig. S1–S6, ESI†). The *m*/*z* peak corresponding to $[M - Cl]^+$ ion was observed in the HRMS spectrum (Fig. S1–S4, ESI†), and elemental analysis confirmed the purity of **Fe1–Fe4**. The FT-IR spectra of **Fe1–Fe4** exhibited a prominent band, 1600–1615 cm^{-1}, which is attributed to the C=N stretching frequency of the attached Schiff base system (Fig. S5, ESI†). Chakravarty and co-workers reported a similar C=N stretching in Fe(III) complexes at ~1605 cm^{-1}.[58,59] Our group recently observed a similar C=N stretching at ~1610 cm^{-1} with Co(III) complexes.[37,60] The UV-Vis. properties of **Fe1–Fe4** were studied in DMSO containing Luria–Bertani (LB) broth bacterial culture media. The UV-Vis. spectra of **Fe1–Fe4** displayed an absorption band between 350 and 490 nm attributed to LMCT from two phenoxide to Fe(III) center.[58,59] The visible light absorption ability of **Fe1–Fe4** might be useful to achieve the light-triggered antibacterial effect of **Fe1–Fe4** under visible light exposure.

Solubility, stability, and lipophilicity

Fe1–Fe4 displayed excellent solubility in acetonitrile, ethanol, methanol, chloroform, DCM, DMF, and DMSO. **Fe1–Fe4** were sparingly soluble in water and had low solubility in hydrocarbons. The stability of any potential drug is very important for its delivery and effectiveness.[10,15] Thus, the stability of **Fe1–Fe4** was determined in Luria–Bertani media under continuous visible light exposure using UV-Vis. spectroscopy (Fig. S7, ESI†). The UV-Vis. spectra of **Fe1–Fe4** in LB broth media did not show any notable change up to 4 h of light irradiation, indicating significant photostability of these complexes. A similar result was also observed in Nutrient broth (NB) bacterial cell culture medium (Fig. S8, ESI†). Lipophilicity is a critical physicochemical property that significantly influences the cellular uptake and overall bioavailability of drug candidates.[39] The lipophilicity of the **Fe3** complex was experimentally assessed by determining their octanol/water partition coefficients as $\log P_{o/w}$ values (Fig. S9, ESI†). The measured $\log P_{o/w}$ value for **Fe3** was 0.51 ± 0.05. The positive $\log P_{o/w}$ value suggested a passive diffusion-based mechanism for cellular internalization of the complexes.[39]

X-ray crystal structure

To gain insights into the structural features of **Fe1–Fe4**, we obtained the X-ray crystal structure of **Fe3**. The crystals of **Fe3** were grown by the slow evaporation of a saturated 1 : 1 (v/v) methanol : acetone solution. **Fe3** was crystallized as a ClO_4^- salt in a monoclinic system with a $P1/n1$ space group and two molecules in the per unit cell (Fig. 1c and S6, ESI†). Selected crystallographic data, selected bond distances, and bond angles are given in Tables S1 and S2, ESI.† The structure of the complex revealed a distorted octahedral N_4O_2 coordination around Fe(III) center, in which the N,N,N-donor dipicolylamine and the O,N,O-based Schiff base were attached in a meridional manner to the metal. The obtained crystal structure of **Fe3** was similar to previously reported Fe(III) complexes with a similar coordination sphere.[61] The O,N,O donor Schiff base ligand was attached to the Fe(III) center *via* two phenolic oxygen atoms and one nitrogen atom. The bond lengths for Fe–O5 and Fe–O6 were found to be 1.91 and 1.93 Å, respectively (Table S2†). The obtained bond lengths were almost similar to the previously reported crystal structure.[61] The Fe–N distances varied from 2.09 to 2.14 Å. The Fe–N2 2.13 Å bond distance was longer compared to the other Fe–N bond lengths were a bit shorter than in the previously reported complex (2.22 Å).[61] The two sides of the nitrogen atom (N2 and N4) bind with the Fe(III) centre at an angle of 176.8°, which were slightly higher than previously reported, 166.0°.[61]

Computational study

To obtain the energy-minimized structures of the **Fe1–Fe4** as well as the frontier orbitals, density functional theory (DFT) calculations were performed using the Gaussian 16 package.[62] The B3LYP function and the combinatorial basis set (LANL2DZ for Fe and 6-31g* for all other atoms) have been employed to optimize these complexes in this investigation.[62–64] The optimized structure of the complexes was obtained through energy minimization to gain a sensitive and stable system. The frequency calculation was further employed to ensure local minima at the same level of theory.[62–64] The optimized structure of **Fe1–Fe4** indicate that the Fe(III) center is attached in a distorted octahedral geometry with two chelating, N,N,N donor (dpa or Fc-dpa), and O,N,O donor Schiff bases ligands (Fig. 2). The frontier molecular orbitals (FMOs) analysis revealed significant contributions from both the metal centre and coordinated tridentate ligands, as given in Fig. 2a. In case of **Fe1** and **Fe3**, the highest occupied molecular orbital (HOMO) was primary localized on the O,N, O-donor Schiff. However, in the case of **Fe2** and **Fe4**, the HOMO was mainly localized around the attached ferrocene moiety in Fc-dpa. The shift in HOMO localization indicates that, the incorporation of ferrocene moiety into the in dpa framework altered the electronic distribution in the complexes. The lowest unoccupied molecular orbital (LUMO) for **Fe1**, **Fe2**, and **Fe4** was mainly localized over the Fe(III) center and O, N,O-donor Schiff base, whereas in **Fe3**, the LUMO was primarily located on the dpa ligand. These observations underscored the role of ligand structure in modulating the electronic properties of the complexes. The low HOMO–LUMO gap (ΔE_g ~ 2.06–2.32 eV) for the complexes **Fe1–Fe4** corresponded to absorption energies falling within the visible range of the spectrum. These results suggested that electronic transition from the HOMO to the LUMO can be efficiently induced upon photoirradiation, potentially initiating photosensitization, the pro-

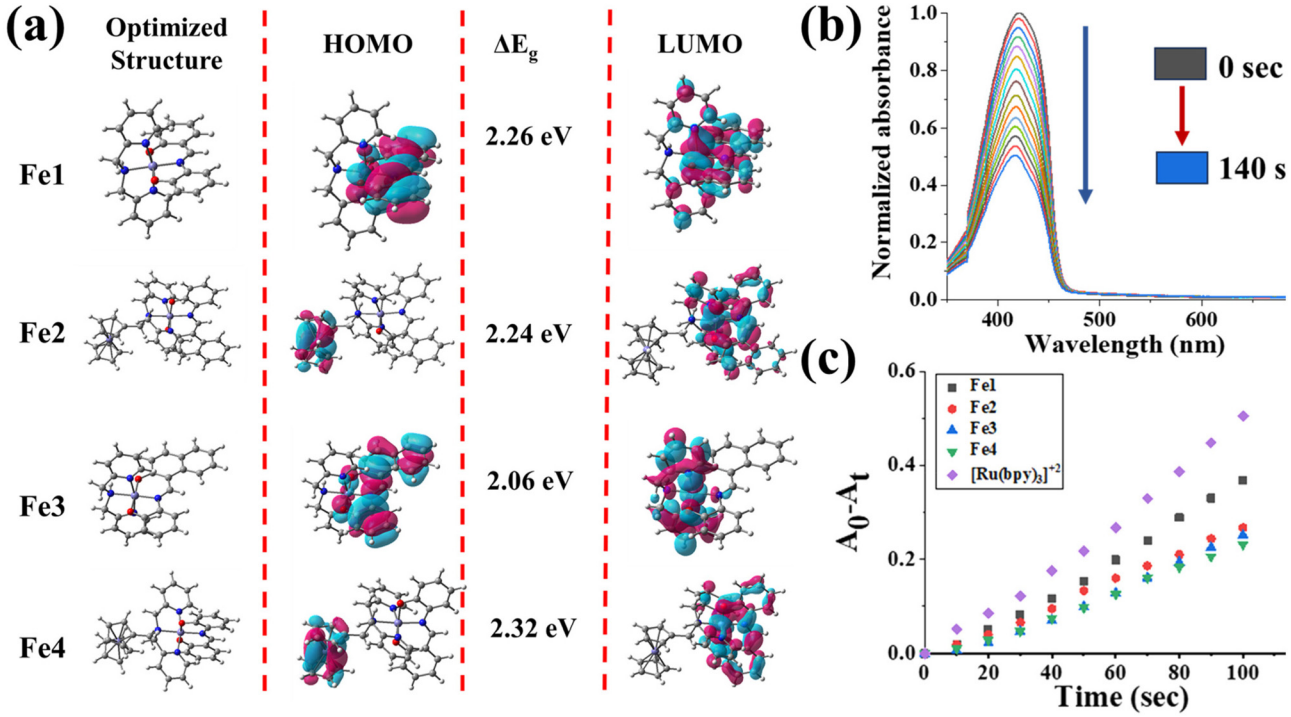

Fig. 2 (a) DFT energy-optimized structures, HOMO, LUMO of **Fe1–Fe4**. (b) Singlet oxygen generation by **Fe1** (10 μM) under visible light irradiation (400–700 nm, 10 J cm^{-2}), monitored by the decrease in DPBF-based absorption peaks. (c) Comparison of $^1O_2$ generation between **Fe1–Fe4** and [Ru(bpy)$_3$]Cl_2 from the decline in the DPBF-based absorbance peak at 417 nm.

cesses conducive to aPDT.[11,37,38] Overall, DFT calculation indicated that **Fe3** might be a better photosensitizer than the other three complexes (**Fe1**, **Fe2**, and **Fe4**). The energy differences between HOMO and LUMO (ΔE_g) for **Fe1–Fe4**, indicating their FMOs topologies, are shown in Fig. 2a.

Generation of ROS by Fe1–Fe4

Singlet oxygen ($^1O_2$) production can induce oxidative stress, membrane dispersion, protein denaturation, and DNA damage in aPDT.[37–41] Furthermore, compared to conventional antibiotics, aPDT is less likely to cause bacterial resistance due to its novel action involving $^1O_2$-triggered damage of cellular components in bacteria.[24,30–32] Many Fe(III) based complexes have exhibited anticancer PDT activity through $^1O_2$ generation *via* a type-II mechanism.[58,59,64–67] Thus, to assess **Fe1–Fe4**'s suitability as aPDT agents, we studied their $^1O_2$ production efficiency. 1,3-diphenylisobenzofurane (DPBF) was employed as a $^1O_2$ probe to ascertain whether **Fe1–Fe4** could produce $^1O_2$.[11,24] In the absence of light, **Fe1–Fe4** (10 μM) exhibited negligible $^1O_2$ generation. However, upon light irradiation (10 J cm^{-2}, 400–700 nm), a time-dependent decrease in DPBF absorbance was observed in PBS–DMSO (99 : 1 v/v), confirming their ability to generate $^1O_2$ under light conditions (Fig. 2b and c, and S10, ESI†). This result was also validated by another $^1O_2$ probe, 9,10-diphenyl anthracene (DPA) where **Fe3** displayed $^1O_2$ generation upon light irradiation (10 J cm^{-2}, 400–700 nm) (Fig. S11, ESI†). These findings indicate that the light-activated generation of $^1O_2$ might lead to the inactivation of bacterial cells *via* a type-II PDT pathway. The quantum yield (Φ_Δ) for singlet oxygen generation by **Fe1–Fe4** was evaluated using [Ru(bpy)$_3$]Cl_2 as the standard photosensitizer. The $^1O_2$ quantum yield of **Fe1–Fe4** was observed between the range of 0.10–0.16 (Fig. 2c). Furthermore, the generation of $^{\bullet}OH$ by **Fe1–Fe4** was evaluated with methylene blue (MB), an $^{\bullet}OH$ probe. Upon light irradiation, a gradual decrease in the characteristic absorbance of MB (10 μM) at around ~670 nm was observed in a H_2O–DMSO (99 : 1 v/v) solution containing **Fe1–Fe4** (2 μM) (Fig. S12, ESI†), indicating efficient $^{\bullet}OH$ production. Overall, the above findings suggest that **Fe1–Fe4** possess promising potential for application in aPDT, through the type-I and type-II reactive oxygen species (ROS) generation pathways.

Antibacterial activity and MIC value

The notable photo-physical and light-triggered $^1O_2$ generation capability of **Fe1–Fe4** prompted us to investigate their aPDT efficacy. Consequently, their antibacterial activity was explored against *S. aureus and E. coli* bacteria both in the dark and following exposure to low-energy visible light (10 J cm^{-2}, 400–700 nm). Without light irradiation, **Fe1–Fe4** did not exhibit any antibacterial efficacy against *S. aureus* and *E. coli* bacteria. However, under light exposure against *S. aureus* bacteria, all the complexes showed remarkable antibacterial activity; **Fe1** showed inhibition zones of 3.0 mm and 2.8 mm at concentrations of 2 μg mL^{-1} and 1 μg mL^{-1}, respectively in the case of **Fe2**, clear zone of inhibition was observed of *ca.* 4.4 mm diameter at 2 μg mL^{-1} concentration, whereas on

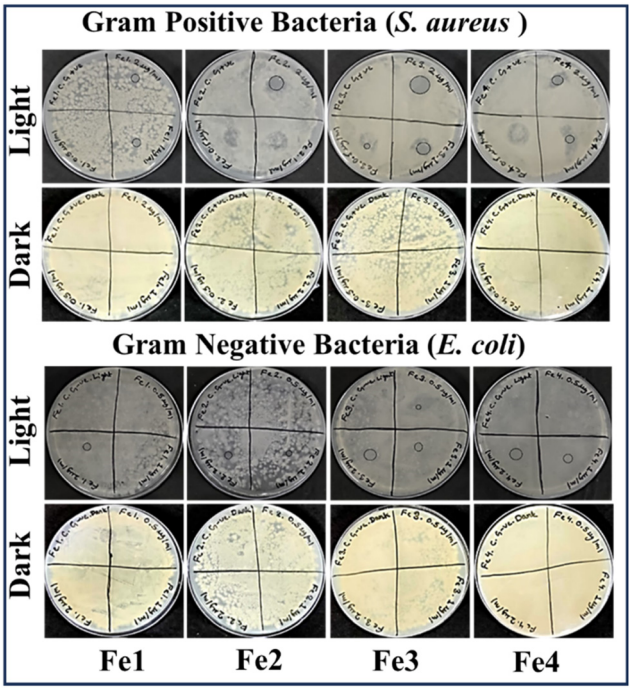

Fig. 3 Light-induced inhibition effect of the **Fe1–Fe4** against *S. aureus* and *E. coli* bacteria.

reducing the concentration to 0.5–1 μg mL^{-1}, a clear zone of inhibition was not observed (Fig. 3). Furthermore, **Fe3** presented zones of inhibition of *ca.* 6.6 mm, 4.5 mm, and 1.3 mm diameter with 2, 1, and 0.5 μg mL^{-1} concentrations, respectively. **Fe4** showed inhibition zones at 2 and 1 μg mL^{-1} concentrations of 3.8 mm and 2.9 mm diameters, respectively (Fig. 3). Overall, **Fe3** showed a higher zone of inhibition as compared to other complexes against *S. aureus* (Fig. 3). Furthermore, the light-triggered antibacterial responses of **Fe1–Fe4** were also evident against Gram-negative (*E. coli*) bacteria. For example, **Fe1** at 2 μg mL^{-1} concentration produced an inhibition zone at 2.3 mm. **Fe2** showed zone of inhibition activity at 2 μg mL^{-1} and 1 μg mL^{-1} with an inhibition zone of 2.5 and 1.8 mm, respectively (Fig. 3). However, **Fe3** presented inhibition activity at 2, 1, and 0.5 μg mL^{-1} concentration, showing zone of inhibition of 4.8 mm, 3.4 mm, and 1.7 mm, respectively (Fig. 3). Complex **Fe4** exhibiting zones of inhibition measuring 4.7 mm and 3.3 mm at concentrations of 2 μg mL^{-1} and 1 μg mL^{-1}, respectively. Similar to the above result, complex **Fe3** also showed a better zone of inhibition against *E. coli*.

Furthermore, the minimum inhibitory concentration (MIC) values were also determined against *S. aureus and E. coli* bacteria. Under light, complexes **Fe1–Fe4** demonstrated MICs of 1.0, 1.0, 0.2, and 0.5 μg mL^{-1} against *S. aureus*, respectively (Table 1). Against *E. coli* bacteria, **Fe1–Fe4** exhibited significant antibacterial activity with 2.0, 1.0, 0.5, and 1.0 μg mL^{-1} MICs, respectively (Table 1). Under dark conditions, complexes **Fe1** and **Fe2** do not exhibit any antibacterial efficacy against both *S. aureus* and *E. coli* bacteria. **Fe3**, however, showed antibacterial activity against *E. coli* with a 2 μg mL^{-1} MIC value in the absence of light (Table 1). Moreover, **Fe4** showed antibacterial activity toward *S. aureus* and *E. coli* with 2 μg mL^{-1} MIC values under the dark conditions.

Table 1 MIC values (μg mL^{-1}) of **Fe1–Fe4** against *S. aureus* and *E. coli* bacteria under dark and light exposure (400–700 nm, 10 J cm^{-2}) (n.a. = no activity)

	Light		Dark	
Complex	*S. aureus*	*E. coli*	*S. aureus*	*E. coli*
Fe1	1	2	n.a.	n.a
Fe2	1	1	n.a.	n.a.
Fe3	0.2	0.5	n.a.	2
Fe4	0.5	1	2	2

Membrane lysis assay

The bacterial membrane is a critical structural component that is often compromised by antibacterial agents. When bacterial membranes' integrity is compromised, they release larger intracellular components such as RNA, DNA, nucleotides, *etc.*[68–71] These nucleotides exhibit strong UV absorption at 260 nm, which can be utilized to monitor membrane damage.[69–71] Therefore, a membrane disruption study was performed by monitoring the variation in absorbance at 260 nm, corresponding to the release of intracellular compounds, disruption of the cell membrane caused by these complexes against *S. aureus* and *E. coli* bacteria.[60,69–71] With *E. coli* under visible light conditions, **Fe1** at 5 μg mL^{-1} showed an increase in the absorbance from 0.26 to 0.33 by the end of 2 hours (*i.e.*, 120 minutes). Upon increasing the concentration of **Fe1** to 15 and 25 μg mL^{-1}, respectively, the absorbance changes from 0.32 to 0.53 and 0.41 to 0.96 by the end of 2 hours (Fig. 4). **Fe2** at 5 μg mL^{-1} concentration also showed an increase from 0.40

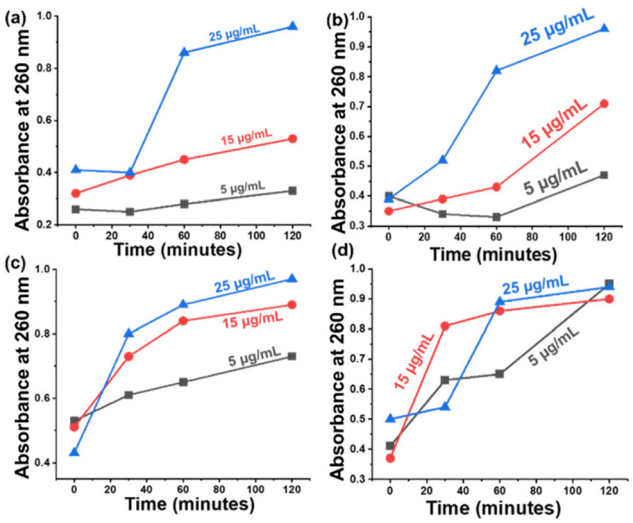

Fig. 4 Membrane lysis assay at 5, 15, and 25 μg mL^{-1} for complexes (a) **Fe1**, (b) **Fe2**, (c) **Fe3**, and (d) **Fe4** against *E. coli*.

to 0.47 at the end of 2 hours, whereas upon increasing the concentration to 15 and 25 μg mL^{-1}, the absorbance increased from 0.35 to 0.71 and 0.39 to 0.96, respectively (Fig. 4). **Fe3**, at a concentration of 5 μg mL^{-1}, showed an increase in absorbance from 0.53 to 0.73, whereas upon increasing the concentration to 15 and 25 μg mL^{-1}, the absorbance increased from 0.51 to 0.89 and 0.43 to 0.97 (Fig. 4). For complex **Fe4**, at 5 μg mL^{-1}, the absorbance increased from 0.41 to 0.95, whereas upon increasing the concentrations to 15 and 25 μg mL^{-1}, the absorbance shifted from 0.37 to 0.9, and 0.5 to 0.94, for activity of complexes against *E. coli* (Fig. 4). Overall, **Fe1** and **Fe2** showed comparatively lower cell membrane damage at lower concentrations, which, however, significantly increased with higher concentrations (Fig. 4). For **Fe3** and **Fe4**, even at low concentration (5 μg mL^{-1}), comparatively higher membrane lysis was observed, which increases with increasing concentrations.

For *S. aureus*, under visible light irradiation, **Fe1** at 5 μg mL^{-1} showed an increase in absorbance from 0.01 to 0.03, whereas at increasing concentrations of 15 and 25 μg mL^{-1}, 0.00 to 0.08, and 0.05 to 0.23 (Fig. 5). **Fe2**, on the other hand, at 5 μg mL^{-1}, showed an increase from 0.00 to 0.04, whereas at 15 and 25 μg mL^{-1}, showed an increase in absorbance from 0.02 to 0.12, and 0.00 to 0.10 (Fig. 5). **Fe3** at a concentration of 5 μg mL^{-1} from 0.01 to 0.03, whereas upon increasing concentration to 15 and 25 μg mL^{-1}, the change in absorbance of 0.02 to 0.09 and 0.02 to 0.16 (Fig. 5). For **Fe4**, at lower concentrations of 5 μg mL^{-1}, the absorbance change was observed from 0.01 to 0.16, whereas upon increasing the concentration to 15 and 25 μg mL^{-1}, the absorbance changes of 0.16 to 0.51 and 0.08 to 0.44 (Fig. 5). These findings suggested a concentration-dependent membrane lysis against *S. aureus*. **Fe1**, **Fe2**, and **Fe3** showed lower membrane lysis than **Fe4**. Overall, against *E. coli*, **Fe3** and **Fe4** showed the maximum antibacterial efficacy, whereas against *S. aureus*, **Fe2** and **Fe4** showed the maximum antibacterial activity. The complexes showed comparatively higher membrane lysis against Gram-negative bacteria. The membrane lysis study under light conditions suggested the potential of Fe(III) complexes to induce significant disruption in membrane integrity against both Gram-positive and Gram-negative bacteria.

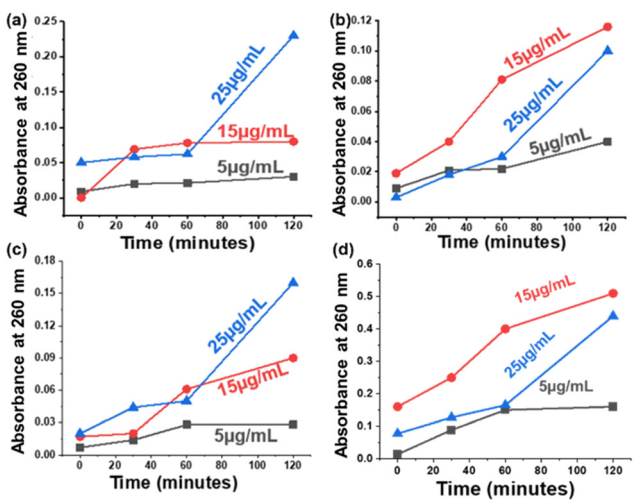

Fig. 5 Membrane lysis assay at 5, 15, and 25 μg mL^{-1} for complexes (a) **Fe1**, (b) **Fe2**, (c) **Fe3**, and (d) **Fe4** against *S. aureus*.

Conclusions

In summary, we successfully synthesized and characterized four Fe(III) complexes derived from dpa/Fc-dpa and structurally varied Schiff bases. **Fe1–Fe4** exhibited absorption bands in the visible range, suggesting that they could function as photosensitizers for aPDT applications under visible light (400–700 nm) exposure. The crystal structure of **Fe3** revealed the distorted octahedral structure around Fe(III) center. The computational studies provided an insight into the FMOs and the energy gap between HOMO and LUMO ($E_g = E_{LUMO} - E_{HOMO}$) of **Fe1–Fe4** indicating their potential to act as a good aPDT agent. Moreover, in DPBF study, **Fe1–Fe4** significantly reduced the absorption intensity of DPBF-based absorption peaks when exposed to visible light, indicating their efficient $^1O_2$ production abilities. Moreover, these complexes also displayed $^{\bullet}OH$ production in the presence of visible light exposure. Furthermore, **Fe1–Fe4** displayed potent efficacy in killing both Gram-positive (*S. aureus*) and Gram-negative (*E. coli*) bacteria with minimum inhibitory concentrations (MICs) as low as 0.2 μg mL^{-1} under 400–700 nm visible light. **Fe1–Fe4** exhibited superior membrane lysis performance against *S. aureus* and *E. coli* under light. In the absence of light, these complexes did not show significant antibacterial activity, suggesting that **Fe1–Fe4** could be useful as aPDT agents. Overall, the findings suggest that the photo-responsive, Fe(III) complexes hold promise as next next-generation agent for aPDT applications. Furthermore, this study expands the potential of 3d metal-based complexes in the development of effective antibacterial agents for aPDT application.

Author contributions

S. B. has formulated the concept and studies. I. S. carried out the synthesis and characterization, and in-solution studies of the complexes. R. K. carried out the Crystallography and DFT calculations. The antibacterial experiments were performed by R. R. and P. D. All authors have contributed to the writing of the manuscript and finalized this version of the manuscript.

Conflicts of interest

There are no conflicts to declare.

Data availability

The data that support the findings of this study are included as part of the electronic ESI.† Crystallographic data for **Fe3** have been deposited at the CCDC under deposition numbers 2455812† and can be obtained from **https://www.ccdc.cam.ac.uk/structures/**.

Acknowledgements

S. B. acknowledges DST, Government of India (DST/INSPIRE/04/2019/000492), for financial support. I. S. thanks the BRNS for the fellowship. R. K. thanks the Ministry of Education, the Government of India, for the PMRF fellowship. We thank Ashish K. Maurya for laboratory management.

References

1 C. Wang, X. Wei, L. Zhong, C. L. Chan, H. Li and H. Sun, *J. Am. Chem. Soc.*, 2025, **147**, 12361–12380.
2 K. J. Forsberg, A. Reyes, B. Wang, E. M. Selleck, M. O. A. Sommer and G. Dantas, *Science*, 2012, **337**, 1107–1111.
3 J. L. Martínez, *Science*, 2008, **321**, 365–367.
4 C. J. Murray, K. S. Ikuta, F. Sharara, L. Swetschinski, G. R. Aguilar, A. Gray, C. Han, C. Bisignano, P. Rao, E. Wool, S. C. Johnson, A. J. Browne, M. G. Chipeta, *et al.*, *Lancet*, 2022, **399**, 629–655.
5 M. E. A. de Kraker, A. J. Stewardson and S. Harbarth, *PLoS Med.*, 2016, **13**, e1002184.
6 J. O'Neill, Tackling drug-resistant infections globally: final report and recommendations, in *Review on Antimicrobial Resistance*, London, 2016.
7 M. Naghavi, S. E. Vollset, K. S. Ikuta, L. R. Swetschinski, A. P. Gray, E. E. Wool, G. R. Aguilar, T. Mestrovic, G. Smith, C. Han, R. L. Hsu, J. Chalek, D. T. Araki, E. Chung, C. Raggi, A. G. Hayoon, N. D. Weaver, P. A. Lindstedt, A. E. Smith, U. Altay, N. V. Bhattacharjee, K. Giannakis, F. Fell, B. McManigal, N. Ekapirat, J. A. Mendes, T. Runghien, O. Srimokla, A. Abdelkader, S. A. Elsalam, R. G. Aboagye, H. Abolhassani, H. Abualruz, U. Abubakar, H. J. Abukhadijah, S. Aburuz, A. A. Zaid, S. Achalapong, I. Y. Addo, *et al.*, *Lancet*, 2024, **404**, 1199–1226.
8 Z. Si, K. Pethe and M. B. C. Park, *JACS Au*, 2023, **3**, 276–292.
9 A. Frei, A. D. Verderosa, A. G. Elliott, J. Zuegg and M. A. T. Blaskovich, *Nat. Rev. Chem.*, 2023, **7**, 202–224.
10 T. W. Rees, P. Y. Ho and J. Hess, *ChemBioChem*, 2023, **24**, e202200796.
11 I. Singh, A. Upadhyay, A. A. Mandal, S. Saha, P. Pragya, L. Pradhan, M. Nayak, A. Dutta, A. K. Agrawal, S. Mukherjee and S. Banerjee, *J. Med. Chem.*, 2025, **68**, 4453–4465.
12 M. Piksa, C. Lian, I. C. Samuel, K. J. Pawlik, I. D. W. Samuel and K. Matczyszyn, *Chem. Soc. Rev.*, 2023, **52**, 1697–1722.
13 D. A. Heredia, S. R. Martínez, A. M. Durantini, M. E. Pérez, M. I. Mangione, J. E. Durantini, M. A. Gervaldo, L. A. Otero and E. N. Durantini, *ACS Appl. Mater. Interfaces*, 2019, **11**, 27574.
14 A. Sikder, A. Chaudhuri, S. Mondal and N. D. P. Singh, *ACS Appl. Bio Mater.*, 2021, **4**, 4667–4683.
15 C. Weng, Y. L. K. Tan, W. G. Koh and W. H. Ang, *Angew. Chem., Int. Ed.*, 2023, **62**, e202310040.
16 C. Weng, L. Shen, J. W. Teo, Z. C. Lim, B. S. Loh and W. H. Ang, *JACS Au*, 2021, **1**, 1348–1354.
17 L. Jiang, C. R. R. Gan, J. Gao and X. J. Loh, *Small*, 2016, **12**, 3609–3644.
18 J. Wang, P. Zhao, X. Li, H. Fu, X. Yang, G. Wang, Y. Yang, H. Wei, Z. Zhou and W. Liao, *ACS Appl. Bio Mater.*, 2020, **3**, 1580–1588.
19 V. N. Nguyen, Z. Zhao, B. Z. Tang and J. Yoon, *Chem. Soc. Rev.*, 2022, **51**, 3324–3340.
20 A. Frei, A. D. Verderosa, A. G. Elliott, J. Zuegg and M. A. T. Blaskovich, *Nat. Rev. Chem.*, 2023, **7**, 202–224.
21 B. Kar, U. Das, N. Roy and P. Paira, *Coord. Chem. Rev.*, 2023, **474**, 214860.
22 R. Kushwaha and S. Banerjee, *Future Med. Chem.*, 2025, **17**, 1101–1103.
23 J. Karges, *Angew. Chem., Int. Ed.*, 2022, **61**, e202112236.
24 J. Karges, R. W. Stokes and S. M. Cohen, *Trends Chem.*, 2022, **3**, 523–534.
25 J. Karges, H. Chao and G. Gasser, *J. Biol. Inorg. Chem.*, 2020, **25**, 1035–1050.
26 I. Doumi, D. A. Othman, S. Hua, V. Lebrun, F. Meyer and P. Faller, *Chem. Commun.*, 2025, **61**, 7486–7489.
27 B. F. Hohlfeld, B. Gitter, C. J. Kingsbury, K. J. Flanagan, D. Steen, G. D. Wieland, N. Kulak, M. O. Senge and A. Wiehe, *Chem. – Eur. J.*, 2021, **27**, 6440.
28 J. Xu, T. Wang, Z. Fang, Y. Zhu, L. Liu, L. Zhang and Q. Zhan, *Sens. Actuators, B*, 2023, **376**, 133051.
29 K. L. Smitten, P. A. Scattergood, C. Kiker, J. A. Thomas and P. I. P. Elliott, *Chem. Sci.*, 2020, **11**, 8928–8935.
30 A. A. Mandal, A. Upadhyay, A. Mandal, M. Nayak, K. M. Sabeel, S. Mukherjee and S. Banerjee, *ACS Appl. Mater. Interfaces*, 2024, **16**, 28118–28133.
31 S. A. McFarland, A. Mandel, R. Dumoulin-White and G. Gasser, *Curr. Opin. Chem. Biol.*, 2020, **56**, 23–27.
32 K. S. Egorova and V. P. Ananikov, *Organometallics*, 2017, **36**, 4071–4090.
33 V. Singh, G. Ahmed, S. Vedika, P. Kumar, S. K. Chaturvedi, S. N. Rai, E. Vamanu and A. Kumar, *Sci. Rep.*, 2024, **14**, 7595.
34 D. C. Crans and K. Kostenkova, *Commun. Chem.*, 2020, **3**, 104.
35 L. Gourdon, K. Cariou and G. Gasser, *Chem. Soc. Rev.*, 2022, **51**, 1167–1195.
36 A. K. Yadav, V. Singh, R. Kushwaha, D. Dolui, R. Rai, P. Dhar, A. Dutta, B. Koch and S. Banerjee, *ChemBioChem*, 2023, **24**, e202300033.

37 A. Mandal, R. Rai, S. Saha, R. Kushwaha, L. Wei, H. Gogoi, A. A. Mandal, A. K. Yadav, H. Huang, A. Dutta, P. Dhar and S. Banerjee, *Dalton Trans.*, 2023, **52**, 17562–17572.
38 R. Kushwaha, R. Rai, V. Gawande, V. Singh, A. K. Yadav, B. Koch, P. Dhar and S. Banerjee, *ChemBioChem*, 2024, **25**, e202300652.
39 R. Kushwaha, S. Kumari, A. Mishra, A. Upadhyay, A. Rai, M. Nayak, S. Mukherjee and S. Banerjee, *Chem. Commun.*, 2025, DOI: **10.1039/D5CC02340H**.
40 K. Gadar and R. R. McCarthy, *npj Antimicrob. Resist.*, 2023, **1**, 11.
41 S. E. Howson, A. Bolhuis, V. Brabec, G. J. Clarkson, J. Malina, A. Rodger and P. Scott, *Nat. Chem.*, 2012, **4**, 31–36.
42 A. Tovmasyan, I. B. Haberle and L. Benov, *Antioxidants*, 2020, **9**, 972.
43 D. Baecker, Ö. Sesli, L. Knabl, S. Huber, D. O. Höller and R. Gust, *Eur. J. Med. Chem.*, 2021, **209**, 112907.
44 M. Patra and G. Gasser, *Nat. Rev. Chem.*, 2017, **1**, 0066.
45 P. Štěpnička, *Dalton Trans.*, 2022, **51**, 8085–8102.
46 C. Ornelas and D. Astruc, *Pharmaceutics*, 2023, **15**, 2044.
47 A. Nguyen, S. Top, A. Vessières, P. Pigeon, M. Huche, E. A. Hillard and G. Jaouen, *J. Organomet. Chem.*, 2007, **692**, 1219–1225.
48 J. S. McCarthy, T. Rückle, E. Djeriou, C. Cantalloube, D. Ter-Minassian, M. Baker, P. O'Rourke, P. Griffin, L. Marquart, R. Hooft van Huijsduijnen and J. J. Möhrle, *Malar. J.*, 2016, **15**, 469.
49 R. Kushwaha, A. Upadhyay, S. Peters, A. K. Yadav, A. Mishra, A. Bera, T. Sadhukhan and S. Banerjee, *Langmuir*, 2024, **40**, 12226–12238.
50 B. Weber, A. Serafin, J. Michie, C. E. J. Van Rensburg, J. C. Swarts and L. Bohm, *Anticancer Res.*, 2004, **24**, 763–770.
51 G. Gasser, I. Ott and N. Metzler-Nolte, *J. Med. Chem.*, 2011, **54**, 3–25.
52 S. Gadre, M. Manikandan, P. Duari, S. Chhatar, A. Sharma, S. Khatri, J. Kode, M. Barkume, N. K. Kasinathan, M. Nagare, M. Patkar, A. Ingle, M. Kumar, U. Kolthur-Seetharam and M. Patra, *Chem. – Eur. J.*, 2022, **28**, e202201259.
53 M. M, S. Gadre, S. Chhatar, G. Chakraborty, N. Ahmed, C. Patra and M. Patra, *J. Med. Chem.*, 2022, **65**, 16353–16371.
54 K. Mitra, A. Shettar, P. Kondaiah and A. R. Chakravarty, *Inorg. Chem.*, 2016, **55**, 5612–5622.
55 K. Mitra, U. Basu, I. Khan, B. Maity, P. Kondaiah and A. R. Chakravarty, *Dalton Trans.*, 2014, **43**, 751–763.
56 B. Balaji, B. Balakrishnan, S. Perumalla, A. A. Karande and A. R. Chakravarty, *Eur. J. Med. Chem.*, 2015, **92**, 332–341.
57 T. K. Goswami, S. Gadadhar, B. Balaji, B. Gole, A. A. Karande and A. R. Chakravarty, *Dalton Trans.*, 2014, **43**, 11988.
58 T. Sarkar, S. Banerjee and A. Hussain, *RSC Adv.*, 2015, **5**, 29276.
59 S. Saha, D. Mallick, R. Majumdar, M. Roy, R. R. Dighe, E. D. Jemmis and A. R. Chakravarty, *Inorg. Chem.*, 2011, **50**(7), 2975–2987.
60 A. Mandal, R. Rai, A. A. Mandal, P. Dhar and S. Banerjee, *Chem. – Asian J.*, 2024, **19**, e202400943.
61 U. Basu, I. Pant, A. Hussain, P. Kondaiah and A. R. Chakravarty, *Inorg. Chem.*, 2015, **54**, 3748–3758.
62 M. J. Frisch, G. W. Trucks, H. B. Schlegel, G. E. Scuseria, M. A. Robb, J. R. Cheeseman, G. Scalmani, V. Barone, G. A. Petersson, H. Nakatsuji, X. Li, M. Caricato, A. V. Marenich, J. Bloino, B. G. Janesko, R. Gomperts, B. Mennucci, H. P. Hratchian, J. V. Ortiz, A. F. Izmaylov, J. L. Sonnenberg, D. Williams-Young, F. Ding, F. Lipparini, F. Egidi, J. Goings, B. Peng, A. Petrone, T. Henderson, D. Ranasinghe, V. G. Zakrzewski, J. Gao, N. Rega, G. Zheng, W. Liang, M. Hada, M. Ehara, K. Toyota, R. Fukuda, J. Hasegawa, M. Ishida, T. Nakajima, Y. Honda, O. Kitao, H. Nakai, T. Vreven, K. Throssell, J. A. Montgomery Jr., J. E. Peralta, F. Ogliaro, M. J. Bearpark, J. J. Heyd, E. N. Brothers, K. N. Kudin, V. N. Staroverov, T. A. Keith, R. Kobayashi, J. Normand, K. Raghavachari, A. P. Rendell, J. C. Burant, S. S. Iyengar, J. Tomasi, M. Cossi, J. M. Millam, M. Klene, C. Adamo, R. Cammi, J. W. Ochterski, R. L. Martin, K. Morokuma, O. Farkas, J. B. Foresman and D. J. Fox, *Gaussian 16, Revision A.03*, Gaussian, Inc., Wallingford CT, 2016.
63 T. Yanai, D. P. Tew and N. C. Handy, *Chem. Phys. Lett.*, 2004, **393**, 51–57.
64 R. Kushwaha, A. Upadhyay, S. Saha, A. K. Yadav, A. Bera, A. Dutta and S. Banerjee, *Dalton Trans.*, 2024, **53**, 13591–13601.
65 T. Sarkar, A. Bhattacharyya, S. Banerjee and A. Hussain, *Chem. Commun.*, 2020, **56**, 7981.
66 M. Pal, V. Ramu, D. Musib, A. Kunwar, A. Biswas and M. Roy, *Inorg. Chem.*, 2021, **60**, 6283–6297.
67 A. Panwar, M. Pal and M. Roy, *J. Inorg. Biochem.*, 2023, **238**, 112055.
68 F. Chen, J. Moat, D. McFeely, G. Clarkson, I. J. H. Portman, J. P. F. Pardoe, F. Harrison, C. G. Dowson and P. J. Sadler, *J. Med. Chem.*, 2018, **61**, 7330–7344.
69 C. Z. Chen and S. L. Cooper, *Biomaterials*, 2002, **23**, 3359–3368.
70 L. L. Panigrahi, S. Shekhar, B. Sahooa and M. Arakha, *RSC Adv.*, 2023, **13**, 25497–25507.
71 F. Lu, Y. Liu, Y. Dai, G. Zhang and Y. Tong, *RSC Adv.*, 2025, **15**, 6357–6369.